CMS Physics Analysis Summary

Contact: cms-pag-conveners-susy@cern.ch 2019/05/23

Search for top squark pair production in a di-tau final state in proton-proton collisions at $\sqrt{s} = 13$ TeV

The CMS Collaboration

Abstract

A search for the pair production of the supersymmetric partner of the top quark, the top squark, produced in proton-proton collision events at $\sqrt{s} = 13$ TeV is presented in final states containing hadronically decaying tau leptons and large missing transverse momentum. These final states are highly sensitive to high $\tan\beta$ or higgsino-like scenarios in which decays of electroweak gauginos to tau leptons are dominant. The search uses a dataset corresponding to an integrated luminosity of 77 fb^{-1} which was recorded by the CMS detector during 2016 and 2017. No significant excess is observed with respect to the background prediction, and exclusion limits at 95% confidence level are presented in the top squark and lightest neutralino mass plane within the framework of simplified models. It is found that top squark masses up to 1100 GeV are excluded for a nearly massless neutralino.

1 Introduction

Supersymmetry (SUSY) [1–9] is one of the most attractive theories of physics beyond the standard model (SM) providing solutions to various drawbacks of the SM itself. In SUSY models there is a bosonic superpartner for each fermion (and vice versa), the superpartner having the same quantum numbers as its SM partner other than spin. The weakly interacting lightest neutralino, $\widetilde{\chi}_1^0$, can be a dark matter candidate in R-parity conserving SUSY models. The SUSY partners of left- and right-handed top quarks, the top squarks, $\widetilde{\mathrm{t}}_\mathrm{L}$ and $\widetilde{\mathrm{t}}_\mathrm{R}$, mix with each other, resulting in physical states $\widetilde{\mathrm{t}}_1$ and $\widetilde{\mathrm{t}}_2$ (assuming $m_{\widetilde{\mathrm{t}}_1} << m_{\widetilde{\mathrm{t}}_2}$). The top squarks play an important role in stabilizing the Higgs boson mass by cancelling the dominant top quark loop contribution to the Higgs boson mass correction. Thus "natural" SUSY requires that the top squark be either very light, of the order of the electroweak scale, or very heavy [10, 11]. Therefore, there is strong motivation to look for signatures of top squark production.

In this study, we focus on the signal of top squark pair production in a di-tau final state. This probes that part of the parameter space of minimal supersymmetric standard models (MSSMs) in which the electroweak gauginos preferentially couple to third generation fermions, namely tau leptons. The interaction of electroweak gauginos with fermion-sfermion pairs involves both gauge and Yukawa terms [9]. The tau lepton Yukawa coupling can be large for a high value of $\tan\beta$ even if the higgsino component in the electroweak gauginos is relatively small. Moreover, a large value of $\tan\beta$ can make the lighter state of the superpartner of the tau lepton ($\tilde{\tau}_1$) much lighter than the superpartners of the first and second generation leptons. In addition, if gauginos are predominantly higgsino-like, they will preferentially couple to third generation fermion-sfermion pairs. Consequently, in this scenario the chargino, $\widetilde{\chi}_1^\pm$, decays predominantly as $\widetilde{\chi}_1^\pm \to \widetilde{\tau}_1^\pm \nu_\tau$ or $\tau^\pm \widetilde{\nu}_\tau$, and the decay rates in electron and muon channels are greatly reduced. Top squark pair production in the high $\tan\beta$ scenario therefore yields τ lepton-enriched final states [12, 13]. Naturally, there is a substantial loss of sensitivity to SUSY signals in electron and muon channels in this scenario.

We focus on the top squark decays $\widetilde{\mathrm{t}}_1 \to \mathrm{b}\widetilde{\chi}_1^\pm \to \mathrm{b}\widetilde{\tau}_1^\pm \nu_\tau \to \mathrm{b}\tau^\pm \widetilde{\chi}_1^0 \nu_\tau$ and $\widetilde{\mathrm{t}}_1 \to \mathrm{b}\widetilde{\chi}_1^\pm \to \mathrm{b}\tau\widetilde{\nu}_\tau \to \mathrm{b}\tau^\pm \widetilde{\chi}_1^0 \nu_\tau$. The $\widetilde{\chi}_1^0$ is assumed to be the lightest SUSY particle (LSP) and being weakly interacting it leaves no signature in the detector, resulting in a momentum imbalance. Hence, the events of interest contain two tau leptons, two b quarks, and an imbalance in transverse momentum. The decay chains are depicted by the four diagrams in Fig. 1 within the simplified model spectra (SMS) framework [14, 15], assuming the $\widetilde{\chi}_1^\pm$ decays to $\widetilde{\tau}_1$ or $\widetilde{\nu}_\tau$ with equal probability.

This search is performed using proton-proton collision events at a center of mass energy of 13 TeV, recorded by the CMS experiment at the CERN LHC. The data sample corresponds to integrated luminosities of 35.9 fb^{-1} and 41.3 fb^{-1} collected during the 2016 and 2017 operating periods of the LHC, respectively. Signal-like events are characterized by the presence of hadronically decaying tau leptons (τ_h), jets identified as likely to have included b hadrons, and large missing transverse momentum. Contributions from SM processes with the same final state are estimated using a combination of Monte Carlo (MC) simulated samples and data driven techniques.

Searches for top squark pair production have been performed by the CMS [16–23] and ATLAS [24–28] collaborations, establishing limits on top squark masses in the framework of SMS models [14, 15]. However, final states containing hadronically decaying tau leptons have not been much explored in the context of top squark searches. The ATLAS collaboration [29] carried out a search based on 2016 data probing a similar final state, but optimized for a gauge-mediated SUSY breaking scenario with an almost massless gravitino as a source of missing momentum.

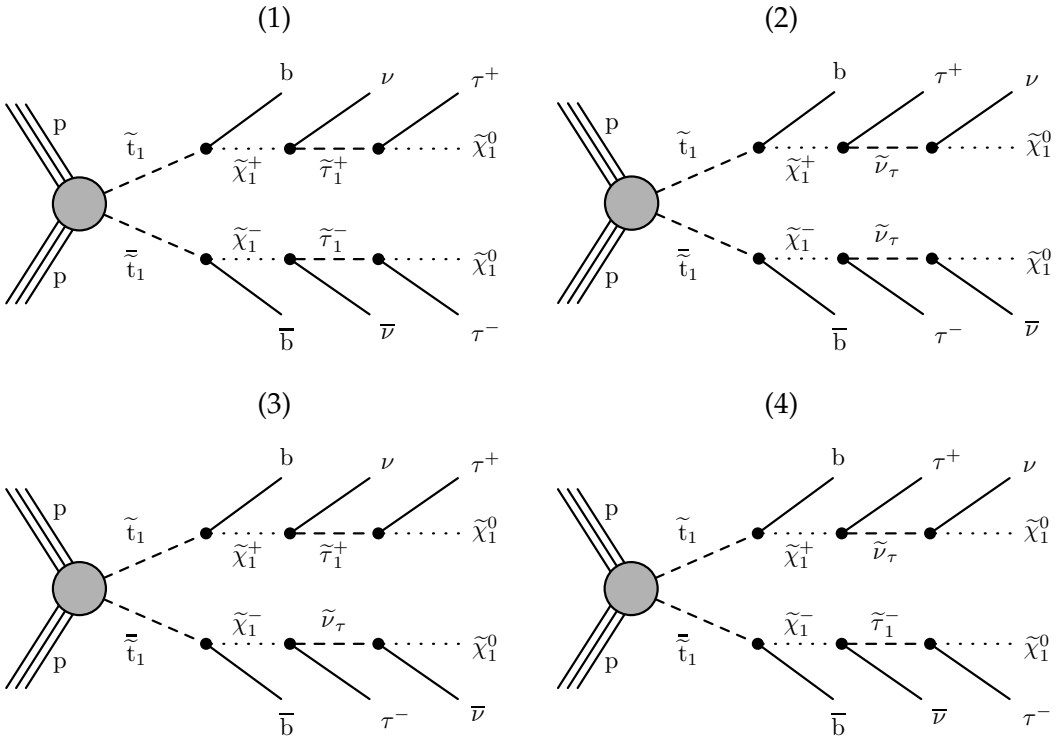

Figure 1: Top squark pair production in proton-proton collisions at the LHC, producing pairs of b quarks and taus accompanied with neutrinos and LSPs in the final state.

We organize the note as follows. A brief description of the CMS detector is presented in Section 2, followed by a description of the event simulation in Section 3, and reconstruction with the CMS detector in Section 4. The event selection and search strategy are detailed in Section 5. We explain the various methods used for background estimation in Section 6, and the results are provided in Section 8. Finally, the analysis is summarized in Section 9.

2 The CMS detector

The central feature of the CMS apparatus is a superconducting solenoid of 6 m internal diameter, providing a magnetic field of 3.8 T. Within the solenoid volume are a silicon pixel and strip tracker, a lead tungstate crystal electromagnetic calorimeter (ECAL), and a brass and scintillator hadron calorimeter (HCAL), each composed of a barrel and two endcap sections. Forward calorimeters extend the pseudorapidity coverage provided by the barrel and endcap detectors. Muons are detected in gas-ionization chambers embedded in the steel flux-return yoke outside the solenoid. A more detailed description of the CMS detector, together with a definition of the coordinate system used and the relevant kinematic variables, can be found in Ref. [30].

Events of interest are selected using a two-tiered trigger system [31]. The first level (L1), composed of custom hardware processors, uses information from the calorimeters and muon detectors to select events at a rate of around 100 kHz within a time interval of less than 4 μs. The second level, known as the high-level trigger, consists of a farm of processors running a version of the full event reconstruction software optimized for fast processing, and reduces the event rate to around 1 kHz before data storage.

3 Monte Carlo simulation

Simulations are used to estimate several of the SM backgrounds. The predictions for signal event rates are also estimated using simulations, based on simplified SUSY signal models.

The pair production of top quarks ($t\bar{t}$) is generated at next-to-leading order (NLO) using POWHEG v2.0 [32]. The MADGRAPH5_aMC@NLO [33] generator is used at leading order (LO) for modeling the Drell-Yan+jets (DY+jets) and W+jets backgrounds, which are normalized to the next-to-next-to-leading order (NNLO) cross sections. The MADGRAPH5_aMC@NLO generator is also used at NLO for simulating the di-boson, single-top, VH, and $t\bar{t}V$ backgrounds (V = W/Z). The parton shower and hadronization are simulated with PYTHIA v8.205 (v8.230 for 2017) [34] using the underlying-event tunes CUETP8M1 [35] and CP5 [36] in 2016 and 2017, respectively. The CMS detector response is modeled using GEANT4 [37], and the simulated events are then reconstructed in the same way as collision data.

Signal processes for top squark pair-production as shown in Fig. 1 are generated at LO using MADGRAPH5_aMC@NLO. The tunes CUETP8M1 and CP2 [36] are used for 2016 and 2017, respectively. The signal cross sections are evaluated using (NNLO) plus next-to-leading-logarithm (NLL) calculations [38–42]. Detector response for the signal events is simulated using the CMS detector simulation (FastSim) [43].

We assume a branching fraction of 50% for each of the two decay modes of the chargino, $\widetilde{\chi}_1^{\pm} \to \widetilde{\tau}_1^{\pm}\nu_\tau$ and $\widetilde{\chi}_1^{\pm} \to \tau^{\pm}\widetilde{\nu}_\tau$. Each of the four diagrams in Fig. 1 therefore contributes 25% of the generated signal events. The masses of supersymmetric particles appearing in the decay chain are determined by the parameterization in Eq. 1:

$$\begin{aligned} m_{\tilde{\chi}_1^{\pm}} - m_{\tilde{\chi}_1^0} &= 0.5\ (m_{\tilde{t}_1} - m_{\tilde{\chi}_1^0}) \\ m_{\tilde{\tau}_1} - m_{\tilde{\chi}_1^0} &= x\ (m_{\tilde{\chi}_1^{\pm}} - m_{\tilde{\chi}_1^0}) \\ x &= [0.25,\ 0.5,\ 0.75] \\ m_{\tilde{\nu}_\tau} &= m_{\tilde{\tau}_1} \end{aligned} \tag{1}$$

In this parameterization, the chargino mass is set to be the mean of the top squark and $\tilde{\chi}_1^0$ masses, and the masses of the leptonic superpartners are set by the value of x. The kinematic properties of the final state therefore depend on the choice of x.

- $x = 0.25$: The mass of the lepton superpartner is closer to that of the $\tilde{\chi}_1^0$ than that of the $\tilde{\chi}_1^{\pm}$. Hence, the first diagram in Fig. 1 produces lower energy tau leptons than the second. The last two diagrams are similar to one another in that there is typically a large difference in energy between the two tau leptons.
- $x = 0.75$: In this case, the masses of the $\widetilde{\tau}_1^{\pm}$ and the $\widetilde{\chi}_1^{\pm}$ are similar, and hence the first diagram in Fig. 1 produces more energetic tau leptons than the second. The latter two diagrams exhibit the same energy asymmetry as in the case of $x = 0.25$.
- $x = 0.5$: The tau leptons in all four diagrams have similar energies.

Once the contributions from all four diagrams are taken into account, the resultant kinematic properties are very similar for the three different values of x for a given set of chargino and LSP masses.

It is important to note however, that the choice of chargino mass does affect the overall sensitivity. For instance, if the chargino is very close to the top squark in mass then the momenta of the b jets would be reduced and that of the remaining decay products would be increased,

which would result in an increase in the overall sensitivity. On the other hand if the chargino were very close to the LSP in mass, then an overall loss of sensitivity would be expected. Such scenarios are not explored in this note, where the default chargino mass given in Eq. 1 is taken throughout. The polarization of the tau lepton originating from chargino and neutralino decays, which has been found to be useful for studying supersymmetric signals [13], has not been exploited here.

The simulations are corrected for small discrepancies observed with respect to collision data using a number of scale factors. These will be discussed in later sections.

4 Event reconstruction

The particle-flow (PF) algorithm [44] is used to reconstruct each individual particle in an event, with an optimized combination of information from the various components of the CMS detector. The energy of photons is obtained from the ECAL measurement, whereas the momentum of electrons is determined from a combination of the measurement of momentum by the tracker, the energy of matching ECAL deposits, and the energy of all bremsstrahlung photons consistent with originating from the track. The energy of muons is obtained from the curvature of the corresponding track. The energy of charged hadrons is determined from a combination of the momentum measured in the tracker and the matching ECAL and HCAL energy deposits, corrected for zero-suppression effects and for the response function of the calorimeters to hadronic showers. Finally, the energy of neutral hadrons is obtained from the corresponding corrected ECAL and HCAL energies.

Reconstruction of jets is performed by clustering PF candidates using the anti-k_{T} jet algorithm [45, 46] with a distance parameter of $R = 0.4$. Jet momentum is determined as the vectorial sum of all particle momenta in the jet, and is found from simulation to be, on average, within 5 to 10% of the true momentum over the whole p_{T} spectrum and detector acceptance. Additional proton-proton interactions within the same or nearby bunch crossings (pileup) can contribute additional tracks and calorimetric energy deposits, increasing the apparent jet momentum. In order to mitigate this effect, tracks identified as originating from pileup vertices are discarded, and an offset is applied to correct for remaining contributions. Jet energy corrections are derived from simulation studies so that the average measured response of jets becomes identical to that of particle level jets. In situ measurements of the momentum balance in di-jet, photon+jet, Z+jet, and multijet events are used to determine any residual differences between the jet energy scale in data and in simulation, and appropriate corrections are made [47]. Additional selection criteria are applied to each jet to remove those potentially dominated by instrumental effects or reconstruction failures. Jets with $p_{\mathrm{T}} > 20\,\mathrm{GeV}$ and $|\eta| < 2.4$ are used in this analysis.

Jets originating from b quarks are identified as b-tagged jets by using the combined secondary vertex (CSVv2) algorithm [48], which utilizes information from any reconstructed secondary vertex along with various kinematic variables. An operating point is chosen corresponding to a signal efficiency of 70% with a mistagging probability of about 1% for light jets (from up and down quarks, and gluons) and 15% for jets originating from charm quarks.

The momentum resolution for electrons with $p_{\mathrm{T}} \approx 45\,\mathrm{GeV}$ from $\mathrm{Z} \to \mathrm{ee}$ decays ranges from 1.7% to 4.5%. It is generally better in the barrel region than in the endcaps, and also depends on the bremsstrahlung energy emitted by the electron as it traverses the material in front of the ECAL [49]. Electrons with $p_{\mathrm{T}} > 20\,\mathrm{GeV}$ and $|\eta| < 2.4$ are used for this analysis.

Muons are measured with detection planes made using three technologies: drift tubes, cathode strip chambers, and resistive plate chambers. Matching muons to tracks measured in the silicon tracker results in a transverse momentum resolution of 1% in the barrel and 3% in the endcaps, for muons with p_T up to 100 GeV. The p_T resolution in the barrel is better than 7% for muons with p_T up to 1 TeV [50]. This search uses muons with $p_T > 20$ GeV and $|\eta| < 2.4$.

Isolation criteria are imposed on the lepton (electron and muon) candidates to reject leptons originating from hadronic decays. The isolation variable used for this purpose is defined as the scalar sum of the transverse momenta of reconstructed charged and neutral particles within a cone of radius $\Delta R = \sqrt{\Delta\eta^2 + \Delta\phi^2} = 0.3\ (0.4)$ around the electron (muon) candidate track, excluding the lepton candidate, divided by the transverse momentum of the lepton candidate. The effect of pileup is subtracted from the isolation variable using a jet area-based method as described in [51]. The electron and muon candidates passing the aforementioned criteria are used to identify a control region that is used for the estimation of the top quark pair background, as explained in Section 6.1.

The missing transverse momentum vector $\vec{p}_T^{\,\text{miss}}$ is computed as the negative vector sum of the transverse momenta of all the PF candidates in an event, and its magnitude is denoted as p_T^{miss} [52]. The $\vec{p}_T^{\,\text{miss}}$ is modified to account for corrections to the energy scale of the reconstructed jets in the event. Anomalous high-p_T^{miss} events may appear due to a variety of reconstruction failures, detector malfunctions, or backgrounds not originating from collisions (e.g. particles in the beam halo). Such events are rejected by filters that are designed to identify more than 85–90% of the spurious high-p_T^{miss} events with a misidentification rate of less than 0.1% [52]. In order to minimize the effect of extra noise in the ECAL endcap in 2017, forward jets with raw $p_T < 50$ GeV and $< 2.65 < |\eta| < 3.139$ are removed from the calculation of p_T^{miss} in both data and MC.

Vertices reconstructed in an event are required to be within 24 cm of the center of the detector in the z-direction, and to have a transverse displacement from the beam line of less than 2 cm. The vertex with the largest value of summed physics-object p_T^2 is taken to be the primary pp interaction vertex. The physics objects used for this purpose are jets, clustered using the jet finding algorithm [45, 46], with the tracks assigned to the vertex as inputs, and the associated missing transverse momentum, taken as the negative vector sum of the p_T of those jets. More details are given in Section 9.4.1 of Ref. [53].

The Hadrons Plus Strips (HPS) algorithm [54] is used to reconstruct τ_h candidates: tau lepton decays containing one charged hadron and up to two neutral pions, or three charged hadrons. The probability of an electron or muon being misidentified as a τ_h candidate is greatly reduced by combining information from the tracker, calorimeters, and muon chambers. The isolation of the τ_h candidate is determined from the presence of reconstructed particles within a radius of $\Delta R = 0.3$ around the τ_h axis that are not compatible with the decay, and is a useful quantity to distinguish jets from τ_h decays. A multivariate discriminant is calculated from the isolation, lifetime and other information. The τ_h candidates are selected with $p_T > 40$ GeV, $|\eta| < 2.1$, and the "tight" working point of the above discriminant. This working point has an efficiency of ≈50% with a misidentification probability of ≈0.03%. Jets lying within $\Delta R < 0.3$ of a τ_h candidate are rejected to avoid double counting. The "loose" working point, which has an efficiency of ≈65% and a misidentification probability of ≈0.07%, is used for estimating the background from misidentified τ_h candidates.

5 Event selection

A major source of missing momentum in the signal is the weakly interacting neutralinos, which are correlated with the visible objects (in particular the τ_h decays). In contrast, the missing momentum in the SM background processes is primarily due to neutrinos. This difference can be exploited by first constructing the transverse mass m_T, defined in Eq. 2:

$$\begin{aligned} m_T^2(\vec{p}_T^{\,vis}, \vec{p}_T^{\,inv}) &= m_{vis}^2 + m_{inv}^2 + 2(E_T^{vis}E_T^{inv} - \vec{p}_T^{\,vis} \cdot \vec{p}_T^{\,inv}) \ , \\ \text{where} \qquad E_T^2 &= m^2 + p_T^2 \ . \end{aligned} \tag{2}$$

The transverse mass has a maximum at the mass of the parent of the visible (vis) and the invisible (inv) particles.

To account for multiple sources of missing momentum in the signal process, the "stransverse mass" [55, 56] is defined in Eq. 3:

$$m_{T2}(vis1, vis2, p_T^{miss}) = \min_{\vec{p}_T^{\,inv1} + \vec{p}_T^{\,inv2} = \vec{p}_T^{\,miss}} [\max\{m_T^2(\vec{p}_T^{\,vis1}, \vec{p}_T^{\,inv1}), m_T^2(\vec{p}_T^{\,vis2}, \vec{p}_T^{\,inv2})\}] \tag{3}$$

Since the momenta of the individual invisible particles in Eq. 3 is unknown, $\vec{p}_T^{\,miss}$ is divided into two components ($\vec{p}_T^{\,inv1}$ and $\vec{p}_T^{\,inv2}$) in such a way that the value of m_{T2} is minimized. If m_{T2} is computed using the two τ_h candidates as the visible objects, then its upper limit in the signal will be at the chargino mass. This is different from the SM background processes. For example in $t\bar{t}$ events, the upper limit is at the W boson mass. For this analysis, m_{T2} in signal events is calculated with the mass of the invisible particle in Eq. 2 set to zero [57].The total visible momentum of the system is characterized using the quantity H_T, which is defined as the scalar sum of the transverse momenta of all jets and the τ_h candidates. Being a measure of the total energy of the system, H_T is sensitive to the mass of the top squark.

Signal events are selected using di-τ_h triggers, where both the τ_h candidates are required to have $|\eta| < 2.1$, and $p_T > 35$ or 40 GeV, depending on the trigger. The di-τ_h trigger has an efficiency of ≈95% for τ_h candidates that pass the offline selection. For the offline selection, signal events are required to have $p_T^{miss} > 50\,GeV$, $H_T > 100\,GeV$, at least two oppositely charged τ_h candidates with $p_T > 40\,GeV$ and $|\eta| < 2.1$, and at least one b-tagged jet with $p_T > 20\,GeV$ and $|\eta| < 2.4$. The cuts on p_T^{miss} and the number of b-tagged jets (n_b) help to reduce the contributions from DY+jets and SM events comprised uniquely of jets produced through the strong interaction, referred to as multijet events. Distributions of the search variables p_T, m_{T2}, and H_T after these baseline selections are shown in Fig. 2 for data and the predicted background, along with a few representative signal distributions. The background prediction includes $t\bar{t}$, DY+jets, events with misidentified (fake) τ_h, and other rare SM processes. Detailed descriptions of the background estimation methods are presented in Section 6.

Signal events with different top squark and LSP masses become significant in different regions of the phase space. For example, regions with low p_T^{miss}, m_{T2}, and H_T are sensitive to signals with low top squark masses. On the other hand, events with high p_T^{miss}, m_{T2}, and H_T are sensitive to models with high top squark and low LSP masses. In order to obtain the highest sensitivity over the entire phase space, the signal region (SR) is divided into 15 bins which are shown in Fig. 3.

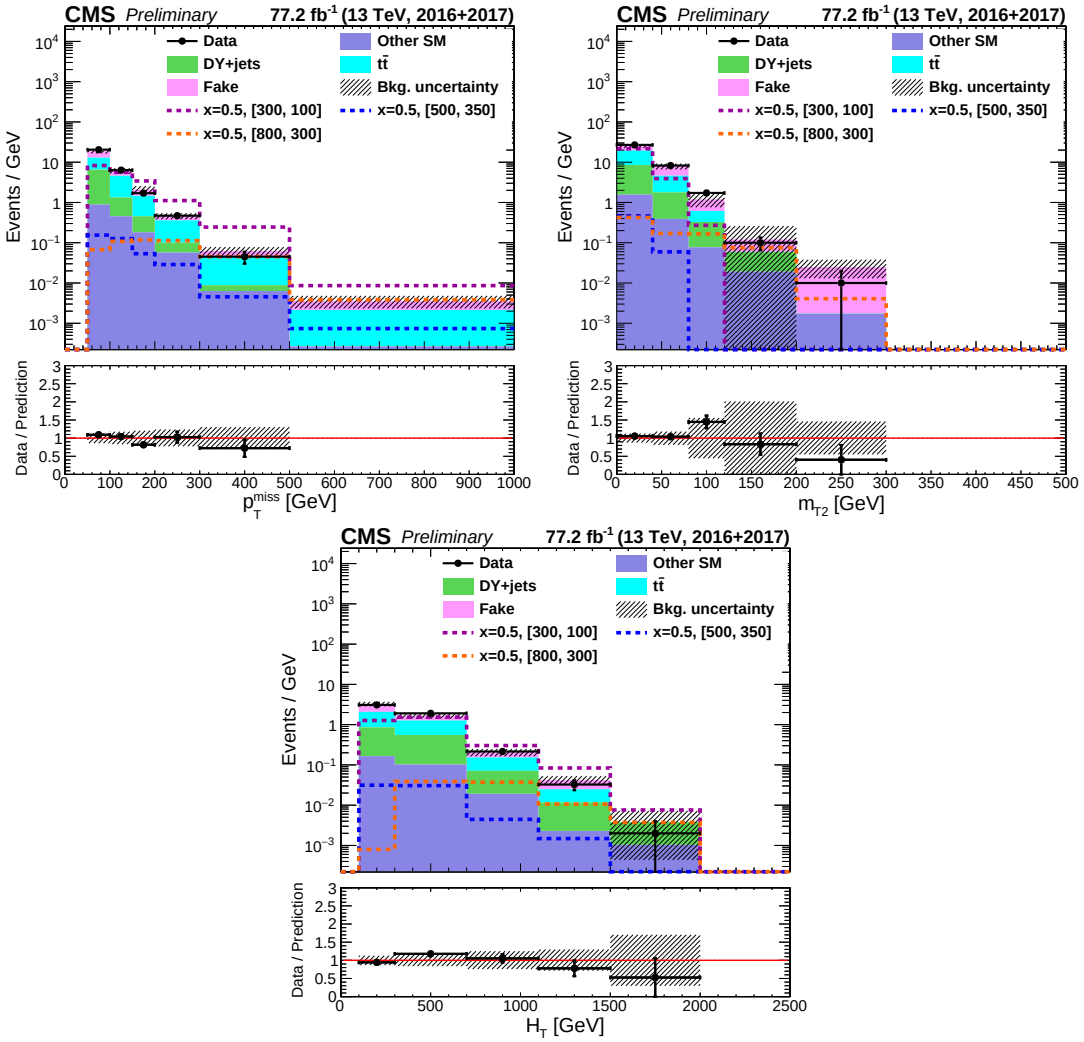

Figure 2: Distributions of the search variables $p_{\mathrm{T}}^{\mathrm{miss}}$, m_{T2}, and H_{T} after baseline selections for data and the predicted background. The distributions for a few representative signal points corresponding to $x = 0.5$ and $[m_{\tilde{\mathrm{t}}_1}, m_{\tilde{\chi}_1^0}]$ = [300, 100] GeV, [500, 350] GeV, and [800, 300] GeV are overlaid.

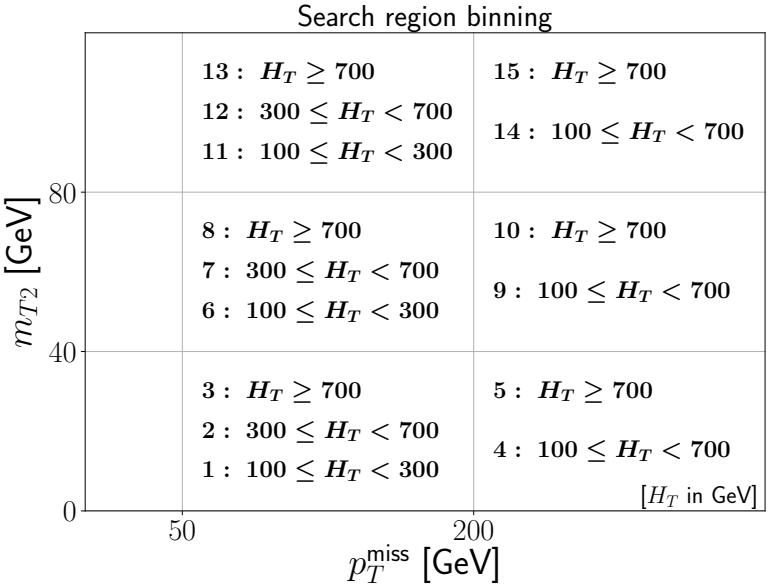

Figure 3: The 15 search regions defined in bins of $p_{\mathrm{T}}^{\mathrm{miss}}$, m_{T2}, and H_{T}.

6 Background estimation

The most significant background is $\mathrm{t\bar{t}}$ production, either with two genuine τ_{h} decays or due to jets being misidentified as τ_{h} candidates. Due to the theoretical imprecision in $\mathrm{t\bar{t}}$ modeling, we estimate the $\mathrm{t\bar{t}}$ contribution using a data-driven method as discussed below. The background contribution from DY events is typically minor in the most sensitive bins, and has been estimated using simulation. The modeling of the Z boson mass and p_{T} spectrum in the LO DY sample can be unreliable, so correction factors for simulated events are derived from DY-enriched dimuon control regions in data and simulation as functions of the Z boson mass and p_{T}. The contribution from multijet events is negligible after the baseline selections. Other less significant backgrounds, such as W+jets, VV, VH, and $\mathrm{t\bar{t}V}$ (V = W/Z) are also obtained from simulation. In the following sections we detail the estimation of the data-driven backgrounds.

6.1 The $\mathrm{t\bar{t}}$ background

As previously mentioned, a data-driven approach [58] is followed to estimate the $\mathrm{t\bar{t}}$ background with two genuine τ_{h} in order to correct for the theoretical imprecision in modeling $\mathrm{t\bar{t}}$ events in the SR. This is performed by multiplying the predicted yields in each SR bin from simulation with correction factors derived in a $\mathrm{t\bar{t}}$-enriched control region (CR). Since the CMS detector can identify electrons and muons with high efficiency, the $\mathrm{t\bar{t}}$-enriched control region is identified by selecting events with an oppositely charged $\mathrm{e}\mu$ pair. These events are selected with $\mathrm{e}\mu$ triggers, and applying the same offline selection as the signal region. These triggers are $\approx 95\%$ efficient for lepton candidates. In addition, in order to avoid possible DY contamination in this CR, events are vetoed if the invariant mass of the $\mathrm{e}\mu$ system lies in the range $60 < m_{\mathrm{e}\mu} < 120\,\mathrm{GeV}$. Other objects such as jets and b-tagged jets are selected using the same kinematic cuts and working points as discussed previously. The definitions of the search variables for this CR are the same as those in the SR, except that the $\mathrm{e}\mu$ pair is used in place of the τ_{h} pair for evaluating the search variables. The purity of $\mathrm{t\bar{t}}$ in the CR (i.e. the fraction of $\mathrm{t\bar{t}}$ events in each search bin) is measured in simulation as $\gtrsim 85\%$, as shown in Fig. 4 (top).

For a given SR bin (i), the scale-factor (SF) is defined as:

$$SF_i = \frac{N^{e\mu\ CR}_{i,\ Data}}{N^{e\mu\ CR}_{i,\ MC}} \quad , \tag{4}$$

where the numerator and the denominator represent the yields in the CR in data and simulation, respectively. The corrected $t\bar{t}$ yield in simulation in each bin of the SR is then obtained as:

$$N^{\tau_h\tau_h\ SR}_{i,\ \text{corr}\ t\bar{t}} = N^{\tau_h\tau_h\ SR}_{i,\ t\bar{t}\ MC} \times SF_i \quad = \frac{N^{e\mu\ CR}_{i,\ Data} \times N^{\tau_h\tau_h\ SR}_{i,\ t\bar{t}\ MC}}{N^{e\mu\ CR}_{i,\ MC}} \quad , \tag{5}$$

where $N^{\tau_h\tau_h\ SR}_{i,\ t\bar{t}\ MC}$ is the prediction from simulated $t\bar{t}$ events in the SR. An alternative way of interpreting this method is to say that we take the $t\bar{t}$ spectrum from a $t\bar{t}$-enriched $e\mu$ CR in data ($N^{e\mu\ CR}_{i,\ Data}$) and extrapolate it to the $\tau_h\ \tau_h$ SR by accounting for the differences between the properties of $\tau_h\ \tau_h$ and $e\mu$ final states with the ratio $N^{\tau_h\tau_h\ SR}_{i,\ t\bar{t}\ MC} / N^{e\mu\ CR}_{i,\ MC}$ from simulation. The SFs in the different search bins, shown in Figure 4 (middle) for both 2016 and 2017, are found to be within $\approx 10\%$ of unity.

In order to cross-check the validity of this method, the same technique is performed in an independent $t\bar{t}$-enriched CR with an oppositely charged $\mu\mu$ pair in the final state. These events are selected with single muon triggers that reach efficiencies of $\approx$ 95%.The event selection for the $\mu\mu$ CR is similar to that for the $e\mu$ CR. This cross check evaluates the effect of possible contamination from DY (the cross-section of $Z/\gamma^* \to \mu\mu$ being much higher than that of $Z/\gamma^* \to \tau\tau \to e\mu$), and is also useful for checking any dependence of the SFs on lepton reconstruction. The differences in the SFs ($SF_i^{e\mu} - SF_i^{\mu\mu}$) shown in Fig. 4 (bottom) are small ($\approx 10\%$ or less), and are taken as a systematic uncertainty on the SFs. These are added in quadrature to the statistical uncertainty on the SFs, and propagated as a contribution to the uncertainty on the final $t\bar{t}$ prediction.

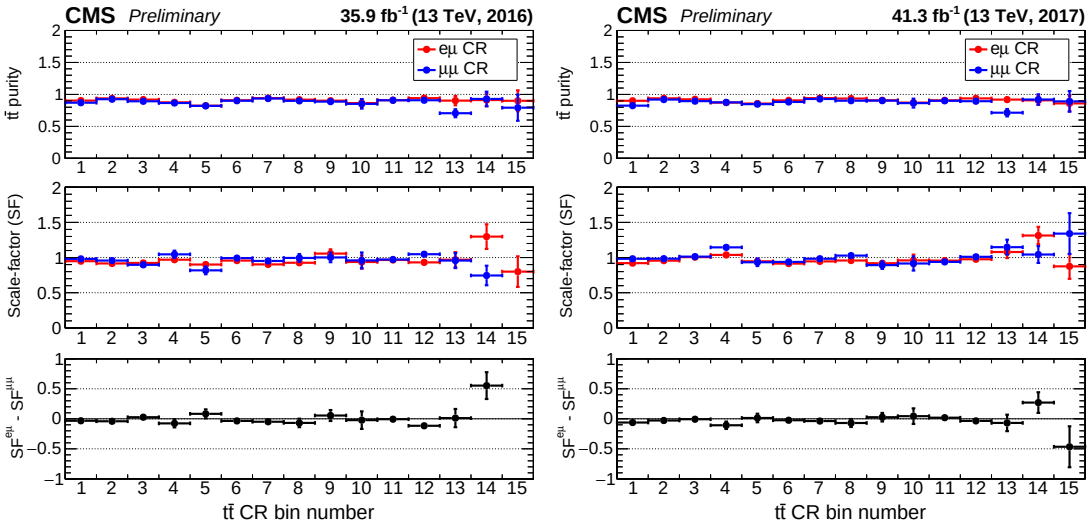

Figure 4: Plots showing the purities (top), scale-factors (middle), and $SF^{e\mu} - SF^{\mu\mu}$ (bottom) in the different bins of the $t\bar{t}$ CR for 2016 (left) and 2017 (right) data.

6.2 Misidentified hadronic tau lepton background

The next largest component of the total background originates from quark or gluon jets being misidentified as a "fake" τ_h candidate. The largest sources of such events in the SR are semileptonic and hadronic $t\bar{t}$ decays. We estimate this contribution to the SR following a strategy [59] that uses the yields in di-τ_h CRs in data, defined by inverting the requirements on the working point of the τ_h identification.

For a genuine τ_h passing the loose identification requirements, we define p as the probability that it also passes the tight identification requirements. We define f as the corresponding probability for a fake τ_h. We then define N_{pf} as the number of di-τ_h events where the τ_h candidate with the highest momentum is genuine and that with the second-highest momentum is fake, with other terms defined similarly. We also define N_{tl} as the number of di-τ_h events where the candidate with the highest momentum passes the tight identification criteria and that with the second highest fails to pass the tight working point but passes the loose criteria, with other terms defined similarly. If N is the total number of events, the following set of equations can be constructed:

$$\begin{aligned}
N &= N_{pp} + N_{fp} + N_{pf} + N_{ff} = N_{tt} + N_{lt} + N_{tl} + N_{ll}, \\
N_{ll} &= (1-p_1)(1-p_2)N_{pp} + (1-f_1)(1-p_2)N_{fp} + (1-p_1)(1-f_2)N_{pf} + (1-f_1)(1-f_2)N_{ff}, \\
N_{lt} &= (1-p_1)p_2N_{pp} + (1-f1)p_2N_{fp} + (1-p_1)f_2N_{pf} + (1-f_1)f_2N_{ff}, \\
N_{tl} &= p_1(1-p_2)N_{pp} + f1(1-p_2)N_{fp} + p_1(1-f_2)N_{pf} + f_1(1-f_2)N_{ff}, \\
N_{tt} &= p_1p_2N_{pp} + f_1p_2N_{fp} + p_1f_2N_{pf} + f_1f_2N_{ff} \quad .
\end{aligned} \tag{6}$$

where the subscripts 1 and 2 on p and f refer to the highest and second-highest momentum τ_h candidates, respectively.

The above equations can be inverted to give the numbers of genuine and fake τ_h candidates in the signal region:

$$\begin{aligned}
N_{tt} &= N_{tt}^{prompt} + N_{tt}^{fake}, \\
\text{where} \quad N_{tt}^{prompt} &= p_1p_2N_{pp}, \\
N_{tt}^{fake} &= f_1p_2N_{fp} + p_1f_2N_{pf} + f_1f_2N_{ff} \quad .
\end{aligned} \tag{7}$$

Here N_{tt}^{prompt} represents the number of events in the signal region with two genuine τ_h candidates in the final state, and N_{tt}^{fake} the number of events in the signal region with one or two fake τ_h candidates.

The probability p is determined using $t\bar{t}$ simulation, with the τ_h candidate being matched to a generated hadronically decaying tau within a cone of radius $\Delta R = 0.3$. The value of p is calculated as the ratio between the number of genuine τ_h jets passing the tight identification criteria and the number passing the loose one. It is evaluated as a function of the tau lepton decay mode and is observed to be about 80% with very little dependence on the p_T of the τ_h. The dependence on the decay mode is observed to be at the 10% level.

The fake rate f is estimated using a multijet-enriched CR in data. This CR is defined by requiring a same-charge τ_h pair satisfying the τ_h selection criteria, and by requiring $p_T^{miss} < 50\,GeV$. The fake rate for a single tau is estimated from this CR using the following two definitions:

$$
\begin{aligned}
f(LL \to TL) &= \frac{\tau_{\mathrm{h}}^{1}(T)\,\tau_{\mathrm{h}}^{2}(L)}{\tau_{\mathrm{h}}^{1}(L)\,\tau_{\mathrm{h}}^{2}(L)} \\
f(TL \to TT) &= \frac{\tau_{\mathrm{h}}^{1}(T)\,\tau_{\mathrm{h}}^{2}(T)}{\tau_{\mathrm{h}}^{1}(T)\,\tau_{\mathrm{h}}^{2}(L)} \quad .
\end{aligned}
\tag{8}
$$

Here, the term $\tau_{\mathrm{h}}^{i}(X)$ denotes the number of events where the highest ($i = 1$) or second highest ($i = 2$) momentum τ_{h} candidate passes the tight ($X = T$) or loose ($X = L$) identification criteria. In each of the two definitions above, the working point of one of the taus in the numerator is changed with respect to the denominator, so they could be expected to yield the same result. However, if the probability of one τ_{h} passing the tight criteria is correlated with the probability of the other to pass, differences may occur. In practice, differences of up to $\approx 10\%$, depending on the p_{T} and the decay mode of the τ_{h}, are observed between the the two definitions. These differences are used to quantify the uncertainty on this method.

The fake rate is measured for different tau lepton decay modes, and is found to be around 35% with a mild dependence on the p_{T} of the τ_{h} candidate. The variations with decay mode are up to the 20% level. It has been found in simulation studies [59] that the fake rate also depends on the flavor of the parton corresponding to the jet which is misidentified as a τ_{h}. Since the jet flavor cannot be reliably determined in data, an additional 15% uncertainty on f is included.

7 Systematic uncertainties

There are several sources of systematic uncertainty that are propagated to the prediction of the final signal and background yields. The most significant is the uncertainty in the modeling of the identification and isolation requirements (ID-iso) [54] of the τ_{h} candidates, estimated to be approximately 10% for all processes in 2016, and 20% in 2017. The other sources of uncertainty affecting all processes, both signal and background, include jet energy scale (JES) and jet energy resolution (JER), τ_{h} energy scale, the effect of unclustered components in calculating $p_{\mathrm{T}}^{\mathrm{miss}}$, pileup reweighting, and b tagging efficiency.

Since the $\mathrm{t\bar{t}}$ contribution in the signal region is obtained by multiplying the simulated yield by a scale factor, defined as the ratio between the number of events in data and simulation, the net effect of several of the uncertainties cancel out. As mentioned earlier, the difference between the $\mathrm{t\bar{t}}$ SFs obtained in the $\mathrm{e}\mu$ and $\mu\mu$ CRs, added in quadrature with the statistical uncertainty on the SF, is taken as the uncertainty on this method. The difference between the two definitions of the fake rate (Eq. 8) is taken to be the uncertainty in its measurement, while the flavor dependence of the fake rate is accounted for by adding an additional 15% uncertainty on the fake rate.

The factorization and renormalization scale (QCD scale) uncertainty is estimated to be less than 6%. The simulation is reweighted to make its pileup distribution identical to that in data. The pileup in data depends on the measured minimum-bias cross section, which is varied by $\pm 2.5\%$ to obtain the uncertainty on this correction. A 2.5% uncertainty on the measured luminosity is considered for 2016, reducing to 2.3% for 2017 data. The uncertainty on the Z p_{T} correction applied to DY events is taken to be 100%. A normalization uncertainty of 15% is assigned to the production cross sections of the background processes that are evaluated directly from simulation [60–66].

Since the detector simulation of the signal is performed using FastSim, the signal yields are corrected to account for the differences in the τ_{h} identification efficiency with respect to the

GEANT4 simulation used for the backgrounds. The statistical error on this correction factor is propagated as its uncertainty. FastSim has a worse $p_{\mathrm{T}}^{\mathrm{miss}}$ resolution compared to the full GEANT4 simulation, because of which the signal yields can be artificially enhanced. To account for this the signal yields are corrected and the uncertainty in the resulting correction to the yield is estimated to be ≈5-10%.

The uncertainties in the signal and background from all sources are presented in Table 1. In each entry, the first and second numbers correspond to the relative uncertainties due to the upward and downward variations of the respective source. These values are the weighted averages of the relative uncertainties in the different search bins with the weights being the yields in the respective bins. The tabulated sources of systematic uncertainties are considered to be uncorrelated.

8 Results

We present the observed and expected yields in all 15 search bins in Table 2 along with their uncertainties. Figure 5 shows the observed data in all of the search bins, compared to the signal and background predictions.

As expected, the dominant background contributions in the sensitive signal bins are from $\mathrm{t\bar{t}}$ and misidentified "fake" τ_{h} events. In cases where the background prediction in a given bin is negligible, the Poissonian upper limit at 68% confidence level (CL) is used for the statistical interpretation. The number of events observed in data is found to be consistent with the SM background prediction, within uncertainties. We set upper limits on signal production at 95% CL using a modified frequentist approach and the $\mathrm{CL_S}$ criterion [67, 68], implemented through an asymptotic approximation of the test statistic [69, 70]. In this calculation all the background and signal uncertainties are modeled as nuisance parameters and profiled in the fit.

Final results are obtained by combining the yields from 2016 and 2017 datasets. The systematic uncertainties due to JEC, factorization and renormalization scales, fake-rate measurement and FastSim $p_{\mathrm{T}}^{\mathrm{miss}}$ correction are taken as correlated, and the rest of the uncertainties are treated as uncorrelated between the two datasets. The results are presented as observed and expected exclusion limits in the top squark and LSP mass plane in Fig. 6. Top squark masses up to 1100 GeV are excluded for a nearly massless LSP. The exclusion limits are insensitive to the choice of x due to the complementary nature of the signal diagrams, as discussed in Section 3.

The most sensitive bins for the higher top squark masses are 14 and 15. The overall data in these two bins is lower than the total background prediction, resulting in the observed limit being higher than the expected one. Hence, even though there is an overall excess (though not statistically significant) in the data, the observed mass limit is stronger than expected as the excesses are primarily in bins 2, 5, 7, and 12, which are less sensitive to the production of high mass top squarks. These bins become more significant for low top squark masses, hence the observed limit is slightly worse than expected in that region. The limits become weaker with decreasing $\Delta m = m_{\tilde{t}_1} - m_{\tilde{\chi}_1^0}$, corresponding to final state particles with lower momentum and hence less sensitivity.

9 Summary

The signature of top squark pair production in final states with two tau leptons has been explored in data collected by the CMS detector during 2016 and 2017, corresponding to integrated luminosities of 35.9 $\mathrm{fb^{-1}}$ and 41.3 $\mathrm{fb^{-1}}$, respectively. The search was performed in a final state

Table 1: Relative systematic uncertainties from different sources on signal and background yields in 2016 and 2017 combined. These values are the weighted (by the yields in the respective bins) averages of the relative uncertainties in the different search bins. For the asymmetric uncertainties, the upper (lower) entry is the uncertainty due to the upward (downward) variation. The numbers in box brackets in the heading indicate the top squark and LSP masses in GeV, respectively.

Uncertainty source	$x = 0.5$ [300, 100]	$x = 0.5$ [500, 350]	$x = 0.5$ [800, 300]	$t\bar{t}$	DY+jets	Other SM	Fake
Signal cross-section	± 6.7 %	± 7.5 %	± 9.5 %	—	—	—	—
FastSim $p_{\mathrm{T}}^{\mathrm{miss}}$ resolution	± 7.4 %	± 10.1 %	± 5.1 %	—	—	—	—
τ_{h} FastSim/FullSim	$+4.4$ % -4.3 %	$+3.7$ % -3.6 %	$+7.9$ % -7.5 %	—	—	—	—
JER	-0.3 % < 0.1 %	-0.8 % < 0.1 %	< 0.1 % < 0.1 %	—	$+0.5$ % $+0.3$ %	-1.0 % -0.3 %	—
JEC	$+0.2$ % -0.6 %	< 0.1 % -0.8 %	$+0.1$ % < 0.1 %	—	$+1.1$ % -1.7 %	$+0.2$ % -1.5 %	—
QCD scale	$+0.6$ % -0.7 %	$+1.9$ % -2.1 %	$+0.3$ % -0.4 %	—	$+4.6$ % -4.4 %	$+3.3$ % -2.6 %	—
τ_{h} ID-iso	$+15.6$ % -14.3 %	$+15.5$ % -14.3 %	$+16.5$ % -15.2 %	$+15.8$ % -14.5 %	$+15.7$ % -14.5 %	$+15.6$ % -14.4 %	—
Pileup	< 0.1 % < 0.1 %	$+0.3$ % -0.2 %	-0.7 % $+0.7$ %	—	-0.2 % $+0.2$ %	-0.9 % $+0.9$ %	—
$p_{\mathrm{T}}^{\mathrm{miss}}$ unclustered energy	-0.2 % -0.8 %	$+1.4$ % -2.0 %	< 0.1 % < 0.1 %	—	$+7.0$ % -1.8 %	$+1.3$ % -1.6 %	—
Background normalization	—	—	—	—	± 15.0 %	± 15.0 %	—
Luminosity	± 2.4 %	± 2.4 %	± 2.4 %	—	± 2.4 %	± 2.4 %	—
b-tagging	$+1.1$ % -1.2 %	$+0.7$ % -0.7 %	$+0.7$ % -0.8 %	—	$+4.7$ % -4.7 %	$+2.4$ % -2.4 %	—
τ_{h} energy scale	$+2.3$ % -3.0 %	$+2.3$ % -3.3 %	$+1.1$ % -0.9 %	$+1.5$ % -1.8 %	$+1.2$ % -1.6 %	$+0.7$ % -1.3 %	—
$\mathrm{t\bar{t}}$ SF	—	—	—	± 2.5 %	—	—	—
Z p_{T} reweighting	—	—	—	—	$+9.1$ % -9.1 %	—	—
τ_{h} fake-rate (parton flavour)	—	—	—	—	—	—	$+16.3$ % -17.5 %
τ_{h} fake-rate ($LL \to TL$ vs. $TL \to TT$)	—	—	—	—	—	—	$+2.7$ % -2.5 %

Table 2: Event yields along with statistical and systematic uncertainties in 2016 and 2017 combined, for different background sources in the 15 search bins as defined in Figure 3. The notation used here is, $\text{yield}^{+\text{stat}+\text{syst}}_{-\text{stat}-\text{syst}}$.

SR bin	$t\bar{t}$	DY+jets	Other SM	Fake	Total bkg.	Data
1	$170.3^{+7.7+21.3}_{-7.7-19.4}$	$97.5^{+10.3+22.1}_{-10.3-20.3}$	$23.0^{+1.9+4.5}_{-1.9-4.4}$	$149.5^{+21.3+5.6}_{-21.3-18.8}$	$440.4^{+24.9+42.2}_{-24.9-42.8}$	417
2	$199.7^{+8.3+22.4}_{-8.3-21.0}$	$154.3^{+11.0+34.5}_{-11.0-32.9}$	$28.7^{+3.0+5.7}_{-3.0-5.4}$	$94.4^{+18.7+22.2}_{-18.7-19.9}$	$477.1^{+23.4+58.9}_{-23.4-55.1}$	559
3	$20.1^{+2.7+2.4}_{-2.7-2.3}$	$19.7^{+3.2+5.7}_{-3.2-4.9}$	$5.1^{+0.8+1.1}_{-0.8-1.6}$	$12.3^{+5.5+4.3}_{-5.5-3.0}$	$57.3^{+7.0+8.9}_{-7.0-7.8}$	49
4	$18.9^{+2.6+2.4}_{-2.6-2.2}$	$4.1^{+1.5+1.0}_{-1.5-1.0}$	$3.8^{+0.8+0.9}_{-0.8-0.9}$	$3.2^{+3.5+1.2}_{-3.5-0.9}$	$30.0^{+4.7+3.8}_{-4.7-3.5}$	28
5	$8.9^{+1.6+1.0}_{-1.6-1.0}$	$0.5^{+6.9+0.1}_{-0.5-0.1}$	$1.6^{+0.4+0.4}_{-0.4-0.3}$	$3.8^{+3.2+1.2}_{-3.2-0.8}$	$14.8^{+7.8+1.8}_{-3.6-1.4}$	22
6	$51.1^{+4.2+5.8}_{-4.2-5.3}$	$36.3^{+5.6+9.0}_{-5.6-9.5}$	$7.8^{+1.3+1.6}_{-1.3-1.8}$	$78.4^{+13.7+12.4}_{-13.7-13.3}$	$173.6^{+15.4+18.8}_{-15.4-19.6}$	169
7	$45.9^{+4.0+5.4}_{-4.0-5.0}$	$14.1^{+3.5+5.8}_{-3.5-4.5}$	$5.2^{+0.8+1.0}_{-0.8-1.1}$	$48.2^{+11.0+11.7}_{-11.0-10.3}$	$113.5^{+12.2+15.4}_{-12.2-13.4}$	133
8	$4.4^{+1.3+0.6}_{-1.3-0.5}$	$4.3^{+1.5+2.0}_{-1.5-1.1}$	$1.4^{+0.4+0.3}_{-0.4-0.3}$	$9.0^{+3.2+3.9}_{-3.2-2.7}$	$19.1^{+3.7+4.6}_{-3.7-3.1}$	23
9	$3.7^{+1.1+0.5}_{-1.1-0.4}$	$0.0^{+7.4+0.0}_{-0.0-0.0}$	$0.7^{+0.3+0.2}_{-0.3-0.2}$	$4.6^{+1.7+2.0}_{-1.7-1.4}$	$9.0^{+7.7+2.1}_{-2.0-1.5}$	4
10	$1.0^{+0.6+0.2}_{-0.6-0.1}$	$0.0^{+7.4+0.0}_{-0.0-0.0}$	$0.5^{+0.2+0.1}_{-0.2-0.1}$	$3.2^{+1.4+1.3}_{-1.4-1.0}$	$4.8^{+7.6+1.3}_{-1.6-1.0}$	1
11	$6.8^{+1.6+1.2}_{-1.6-0.9}$	$2.4^{+1.5+1.3}_{-1.5-0.7}$	$1.4^{+0.4+0.7}_{-0.4-0.3}$	$15.6^{+5.7+4.3}_{-5.7-3.3}$	$26.1^{+6.1+5.0}_{-6.1-3.7}$	30
12	$2.9^{+1.0+0.4}_{-1.0-0.3}$	$8.3^{+2.5+2.7}_{-2.5-1.8}$	$2.1^{+0.3+0.4}_{-0.3-0.4}$	$11.4^{+6.0+1.6}_{-6.0-1.7}$	$24.7^{+6.6+3.6}_{-6.6-2.9}$	41
13	$0.7^{+0.7+0.2}_{-0.5-0.4}$	$2.2^{+0.9+0.6}_{-0.9-0.9}$	$0.7^{+0.2+0.2}_{-0.2-0.2}$	$3.5^{+2.1+1.3}_{-2.1-0.9}$	$7.0^{+2.4+1.5}_{-2.3-1.4}$	6
14	$0.5^{+0.7+0.1}_{-0.5-0.1}$	$0.0^{+7.4+0.0}_{-0.0-0.0}$	$0.6^{+0.2+0.1}_{-0.2-0.1}$	—	$1.1^{+7.5+0.2}_{-0.6-0.2}$	1
15	$0.3^{+0.6+0.1}_{-0.3-0.1}$	$0.4^{+2.9+0.1}_{-0.4-0.1}$	$0.1^{+0.0+0.0}_{-0.0-0.0}$	$1.0^{+0.0+0.4}_{-0.0-0.3}$	$1.8^{+3.0+0.5}_{-0.5-0.3}$	0
Total	$\mathbf{535^{+14+63}_{-14-58}}$	$\mathbf{344^{+23+78}_{-17-73}}$	$\mathbf{83^{+4+16}_{-4-16}}$	$\mathbf{438^{+35+73}_{-35-78}}$	$\mathbf{1400^{+44+125}_{-42-123}}$	**1483**

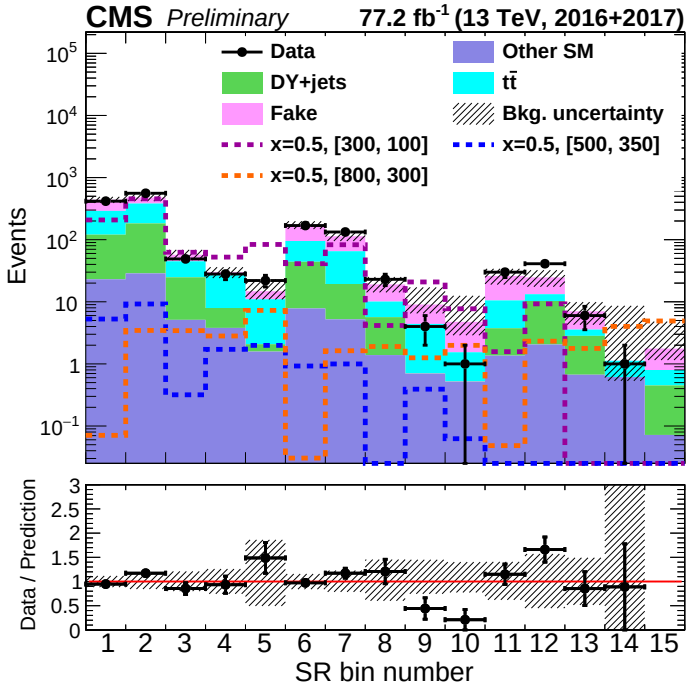

Figure 5: Event yields in the 15 search bins as defined in Figure 3. The yields for a few representative signal points corresponding to $x = 0.5$ and $[m_{\tilde{t}_1}, m_{\tilde{\chi}^0_1}]$ = [300, 100] GeV, [500, 350] GeV, and [800, 300] GeV are overlaid.

containing an oppositely charged hadronic tau lepton pair, at least one jet identified as likely to contain a b hadron, and missing transverse momentum. The dominant standard model backgrounds were found to originate from top quark pair production and processes where jets were misidentified as hadronic tau lepton decays. Data driven techniques were followed to estimate these backgrounds, while other backgrounds were estimated using simulations.

No significant excess was observed, and exclusion limits on top squark masses in terms of neutralino masses were set at 95% confidence level, within the framework of simplfied models where the top squark decays via a chargino to final states including tau leptons. In such models, top squark masses have been excluded up to 1100 GeV for an almost massless LSP, and LSP masses up to 450 GeV have been excluded for a top squark mass of 900 GeV. These results are very useful in probing a region of the supersymmetric parameter space corresponding to high $\tan\beta$ and higgsino-like scenarios.

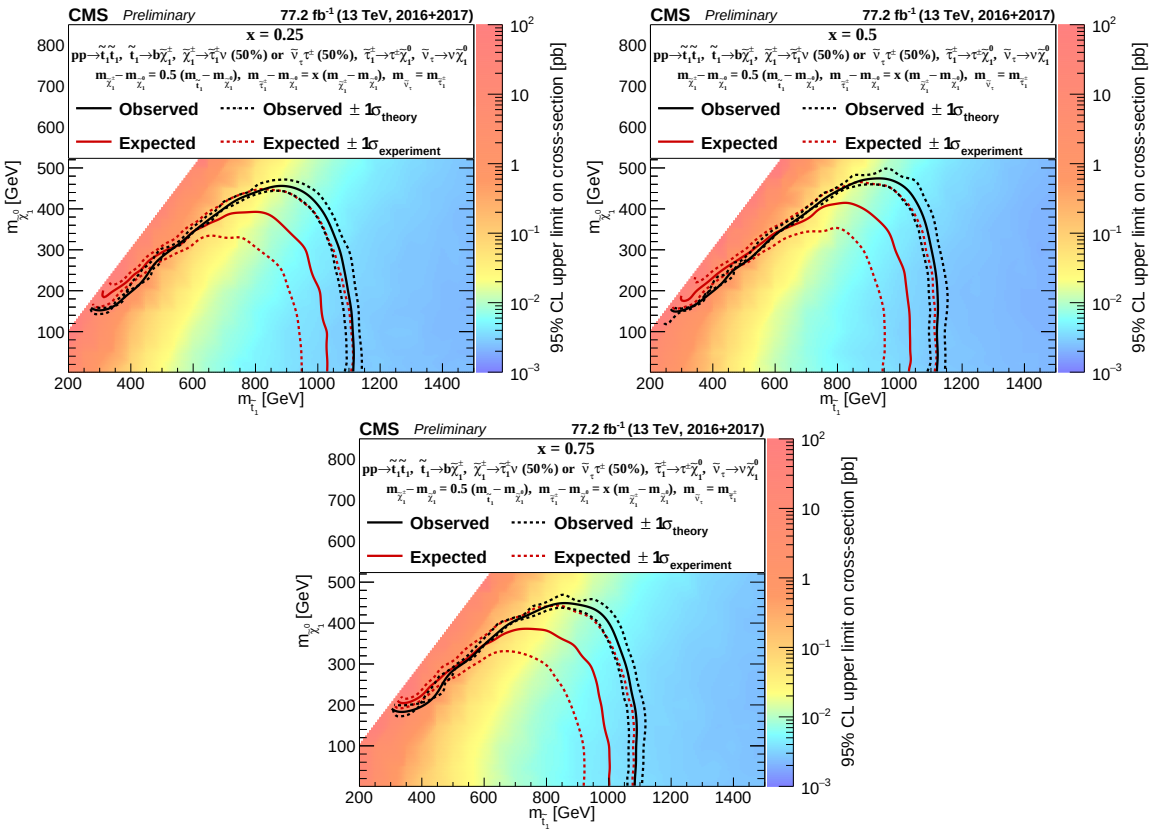

Figure 6: The exclusion limits at 95% CL for the pair production of the top squark decaying in a di-tau final state are displayed in the $m_{\tilde{t}_1}$-$m_{\tilde{\chi}^0_1}$ plane for $x = 0.25$ (top left), 0.5 (top right) and 0.75 (bottom), as described in Equation 1. The black (red) lines represent the observed (expected) limits. The solid lines represent the central values, and the dashed lines the one standard deviation variation due to the theoretical or experimental uncertainties around the central values. The colour shading corresponds to the observed limit on the cross section.

References

[1] P. Ramond, "Dual Theory for Free Fermions", *Phys. Rev.* **D3** (1971) 2415–2418, doi:10.1103/PhysRevD.3.2415.

[2] Yu. A. Golfand and E. P. Likhtman, "Extension of the Algebra of Poincare Group Generators and Violation of p Invariance", *JETP Lett.* **13** (1971) 323–326. [Pisma Zh. Eksp. Teor. Fiz.13,452(1971)].

[3] A. Neveu and J. H. Schwarz, "Factorizable dual model of pions", *Nucl. Phys.* **B31** (1971) 86–112, doi:10.1016/0550-3213(71)90448-2.

[4] J. Wess and B. Zumino, "A Lagrangian Model Invariant Under Supergauge Transformations", *Phys. Lett.* **49B** (1974) 52, doi:10.1016/0370-2693(74)90578-4.

[5] P. Fayet, "Supergauge Invariant Extension of the Higgs Mechanism and a Model for the electron and Its Neutrino", *Nucl. Phys.* **B90** (1975) 104–124, doi:10.1016/0550-3213(75)90636-7.

[6] G. 't Hooft, "Naturalness, chiral symmetry, and spontaneous chiral symmetry breaking", *NATO Sci. Ser. B* **59** (1980) 135–157, doi:10.1007/978-1-4684-7571-5_9.

[7] R. K. Kaul and P. Majumdar, "Cancellation of Quadratically Divergent Mass Corrections in Globally Supersymmetric Spontaneously Broken Gauge Theories", *Nucl. Phys.* **B199** (1982) 36, doi:10.1016/0550-3213(82)90565-X.

[8] H. P. Nilles, "Supersymmetry, Supergravity and Particle Physics", *Phys. Rept.* **110** (1984) 1–162, doi:10.1016/0370-1573(84)90008-5.

[9] S. P. Martin, "A Supersymmetry primer", doi:10.1142/9789812839657_0001,10.1142/9789814307505_0001, arXiv:hep-ph/9709356.

[10] J. R. Ellis, K. Enqvist, D. V. Nanopoulos, and F. Zwirner, "Observables in Low-Energy Superstring Models", *Mod. Phys. Lett.* **A1** (1986) 57, doi:10.1142/S0217732386000105.

[11] R. Barbieri and G. F. Giudice, "Upper Bounds on Supersymmetric Particle Masses", *Nucl. Phys.* **B306** (1988) 63–76, doi:10.1016/0550-3213(88)90171-X.

[12] H. Baer et al., "Collider phenomenology for supersymmetry with large tan Beta", *Phys. Rev. Lett.* **79** (1997) 986–989, doi:10.1103/PhysRevLett.80.642,10.1103/PhysRevLett.79.986, arXiv:hep-ph/9704457. [Erratum: Phys. Rev. Lett.80,642(1998)].

[13] M. Guchait and D. P. Roy, "Using τ polarization as a distinctive SUGRA signature at LHC", *Phys. Lett.* **B541** (2002) 356–361, doi:10.1016/S0370-2693(02)02269-4, arXiv:hep-ph/0205015.

[14] J. Alwall, P. Schuster, and N. Toro, "Simplified Models for a First Characterization of New Physics at the LHC", *Phys. Rev.* **D79** (2009) 075020, doi:10.1103/PhysRevD.79.075020,arXiv:0810.3921.

[15] LHC New Physics Working Group Collaboration, "Simplified Models for LHC New Physics Searches", *J. Phys.* **G39** (2012) 105005, doi:10.1088/0954-3899/39/10/105005,arXiv:1105.2838.

[16] CMS Collaboration, "Search for top squark pair production in pp collisions at $\sqrt{s} = 13$ TeV using single lepton events", *JHEP* **10** (2017) 019, doi:10.1007/JHEP10(2017)019, arXiv:1706.04402.

[17] CMS Collaboration, "Search for top squarks and dark matter particles in opposite-charge dilepton final states at $\sqrt{s} = 13$ TeV", *Phys. Rev.* **D97** (2018), no. 3, 032009, doi:10.1103/PhysRevD.97.032009, arXiv:1711.00752.

[18] CMS Collaboration, "Search for top-squark pair production in the single-lepton final state in pp collisions at $\sqrt{s}$ = 8 TeV", *Eur. Phys. J.* **C73** (2013), no. 12, 2677, doi:10.1140/epjc/s10052-013-2677-2, arXiv:1308.1586.

[19] CMS Collaboration, "Search for direct pair production of scalar top quarks in the single- and dilepton channels in proton-proton collisions at $\sqrt{s} = 8$ TeV", *JHEP* **07** (2016) 027, doi:10.1007/JHEP07(2016)027, 10.1007/JHEP09(2016)056, arXiv:1602.03169. [Erratum: JHEP09,056(2016)].

[20] CMS Collaboration, "Search for top squark pair production in compressed-mass-spectrum scenarios in proton-proton collisions at $\sqrt{s}$ = 8 TeV using the α_T variable", *Phys. Lett.* **B767** (2017) 403–430, doi:10.1016/j.physletb.2017.02.007, arXiv:1605.08993.

[21] CMS Collaboration, "Searches for pair production of third-generation squarks in $\sqrt{s} = 13$ TeV pp collisions", *Eur. Phys. J.* **C77** (2017), no. 5, 327, doi:10.1140/epjc/s10052-017-4853-2, arXiv:1612.03877.

[22] CMS Collaboration, "Search for direct production of supersymmetric partners of the top quark in the all-jets final state in proton-proton collisions at $\sqrt{s} = 13$ TeV", *JHEP* **10** (2017) 005, doi:10.1007/JHEP10(2017)005, arXiv:1707.03316.

[23] CMS Collaboration, "Search for supersymmetry in proton-proton collisions at 13 TeV using identified top quarks", *Phys. Rev.* **D97** (2018), no. 1, 012007, doi:10.1103/PhysRevD.97.012007, arXiv:1710.11188.

[24] ATLAS Collaboration, "Search for direct top squark pair production in final states with two leptons in $\sqrt{s} = 13$ TeV pp collisions with the ATLAS detector", *Eur. Phys. J.* **C77** (2017), no. 12, 898, doi:10.1140/epjc/s10052-017-5445-x, arXiv:1708.03247.

[25] ATLAS Collaboration, "ATLAS Run 1 searches for direct pair production of third-generation squarks at the Large Hadron Collider", *Eur. Phys. J.* **C75** (2015), no. 10, 510, doi:10.1140/epjc/s10052-015-3726-9, 10.1140/epjc/s10052-016-3935-x, arXiv:1506.08616. [Erratum: Eur. Phys. J.C76,no.3,153(2016)].

[26] ATLAS Collaboration, "Search for top squark pair production in final states with one isolated lepton, jets, and missing transverse momentum in $\sqrt{s}$ =8 TeV pp collisions with the ATLAS detector", *JHEP* **11** (2014) 118, doi:10.1007/JHEP11(2014)118, arXiv:1407.0583.

[27] ATLAS Collaboration, "Search for direct top-squark pair production in final states with two leptons in pp collisions at $\sqrt{s} = 8$TeV with the ATLAS detector", *JHEP* **06** (2014) 124, doi:10.1007/JHEP06(2014)124, arXiv:1403.4853.

[28] ATLAS Collaboration, "Search for top squarks in final states with one isolated lepton, jets, and missing transverse momentum in $\sqrt{s} = 13$ TeV pp collisions with the ATLAS detector", *Phys. Rev.* **D94** (2016), no. 5, 052009, doi:10.1103/PhysRevD.94.052009, arXiv:1606.03903.

[29] ATLAS Collaboration, "Search for top squarks decaying to tau sleptons in pp collisions at $\sqrt{s} = 13$ TeV with the atlas detector", *Phys. Rev. D* **98** (Aug, 2018) 032008, doi:10.1103/PhysRevD.98.032008.

[30] CMS Collaboration, "The CMS experiment at the CERN LHC", *JINST* **3** (2008) S08004, doi:10.1088/1748-0221/3/08/S08004.

[31] CMS Collaboration, "The CMS trigger system", *JINST* **12** (2017) P01020, doi:10.1088/1748-0221/12/01/P01020, arXiv:1609.02366.

[32] C. Oleari, "The powheg box", *Nuclear Physics B - Proceedings Supplements* **205-206** (2010) 36 – 41, doi:https://doi.org/10.1016/j.nuclphysbps.2010.08.016. Loops and Legs in Quantum Field Theory.

[33] J. Alwall et al., "The automated computation of tree-level and next-to-leading order differential cross sections, and their matching to parton shower simulations", *JHEP* **07** (2014) 079, doi:10.1007/JHEP07(2014)079, arXiv:1405.0301.

[34] T. Sjostrand, S. Mrenna, and P. Z. Skands, "PYTHIA 6.4 Physics and Manual", *JHEP* **05** (2006) 026, doi:10.1088/1126-6708/2006/05/026, arXiv:hep-ph/0603175.

[35] CMS Collaboration, "Event generator tunes obtained from underlying event and multiparton scattering measurements", *Eur. Phys. J. C* **76** (Dec, 2015) 155. 68 p.

[36] CMS Collaboration, "Extraction and validation of a new set of CMS PYTHIA8 tunes from underlying-event measurements", arXiv:1903.12179.

[37] GEANT4 Collaboration, "GEANT4: A Simulation toolkit", *Nucl. Instrum. Meth.* **A506** (2003) 250–303, doi:10.1016/S0168-9002(03)01368-8.

[38] W. Beenakker, R. Höpker, M. Spira, and P. M. Zerwas, "Squark and gluino production at hadron colliders", *Nucl. Phys. B* **492** (1997) 51, doi:10.1016/S0550-3213(97)00084-9, arXiv:hep-ph/9610490.

[39] A. Kulesza and L. Motyka, "Threshold resummation for squark-antisquark and gluino-pair production at the LHC", *Phys. Rev. Lett.* **102** (2009) 111802, doi:10.1103/PhysRevLett.102.111802, arXiv:0807.2405.

[40] A. Kulesza and L. Motyka, "Soft gluon resummation for the production of gluino-gluino and squark-antisquark pairs at the LHC", *Phys. Rev. D* **80** (2009) 095004, doi:10.1103/PhysRevD.80.095004, arXiv:0905.4749.

[41] W. Beenakker et al., "Soft-gluon resummation for squark and gluino hadroproduction", *JHEP* **12** (2009) 041, doi:10.1088/1126-6708/2009/12/041, arXiv:0909.4418.

[42] W. Beenakker et al., "Squark and gluino hadroproduction", *Int. J. Mod. Phys. A* **26** (2011) 2637, doi:10.1142/S0217751X11053560, arXiv:1105.1110.

[43] A. Giammanco, "The Fast Simulation of the CMS Experiment", *J. Phys. Conf. Ser.* **513** (2014) 022012, doi:10.1088/1742-6596/513/2/022012.

[44] CMS Collaboration, "Particle-flow reconstruction and global event description with the cms detector", *JINST* **12** (2017) P10003, doi:10.1088/1748-0221/12/10/P10003, arXiv:1706.04965.

[45] M. Cacciari, G. P. Salam, and G. Soyez, "The anti-k_t jet clustering algorithm", *JHEP* **04** (2008) 063, doi:10.1088/1126-6708/2008/04/063, arXiv:0802.1189.

[46] M. Cacciari, G. P. Salam, and G. Soyez, "FastJet user manual", *Eur. Phys. J. C* **72** (2012) 1896, doi:10.1140/epjc/s10052-012-1896-2, arXiv:1111.6097.

[47] CMS Collaboration, "Jet energy scale and resolution in the CMS experiment in pp collisions at 8 TeV", *JINST* **12** (2017) P02014, doi:10.1088/1748-0221/12/02/P02014, arXiv:1607.03663.

[48] CMS Collaboration, "Identification of heavy-flavour jets with the CMS detector in pp collisions at 13 TeV", *JINST* **13** (2018) P05011, doi:10.1088/1748-0221/13/05/P05011, arXiv:1712.07158.

[49] CMS Collaboration, "Performance of electron reconstruction and selection with the CMS detector in proton-proton collisions at $\sqrt{s} = 8$ TeV", *JINST* **10** (2015) P06005, doi:10.1088/1748-0221/10/06/P06005, arXiv:1502.02701.

[50] CMS Collaboration, "Performance of the CMS muon detector and muon reconstruction with proton-proton collisions at $\sqrt{s} = 13$ TeV", *JINST* **13** (2018) P06015, doi:10.1088/1748-0221/13/06/P06015, arXiv:1804.04528.

[51] M. Cacciari and G. P. Salam, "Pileup subtraction using jet areas", *Physics Letters B* **659** (2008), no. 1, 119 – 126, doi:https://doi.org/10.1016/j.physletb.2007.09.077.

[52] CMS Collaboration, "Performance of missing transverse momentum reconstruction in proton-proton collisions at $\sqrt{s} = 13$ TeV using the CMS detector", *Submitted to: JINST* (2019) arXiv:1903.06078.

[53] CMS Collaboration, "Technical proposal for the Phase-II upgrade of the Compact Mon Solenoid", CMS Technical proposal CERN-LHCC-2015-010, CMS-TDR-15-02, CERN, 2015.

[54] CMS Collaboration, "Performance of reconstruction and identification of τ leptons decaying to hadrons and ν_τ in pp collisions at $\sqrt{s} = 13$ TeV", *Journal of Instrumentation* **13** (Oct, 2018) P10005–P10005, doi:10.1088/1748-0221/13/10/p10005.

[55] C. G. Lester and D. J. Summers, "Measuring masses of semiinvisibly decaying particles pair produced at hadron colliders", *Phys. Lett.* **B463** (1999) 99–103, doi:10.1016/S0370-2693(99)00945-4, arXiv:hep-ph/9906349.

[56] A. Barr, C. Lester, and P. Stephens, "m(T2): The Truth behind the glamour", *J. Phys.* **G29** (2003) 2343–2363, doi:10.1088/0954-3899/29/10/304, arXiv:hep-ph/0304226.

[57] A. J. Barr and C. Gwenlan, "The Race for supersymmetry: Using m(T2) for discovery", *Phys. Rev.* **D80** (2009) 074007, doi:10.1103/PhysRevD.80.074007, arXiv:0907.2713.

[58] CMS Collaboration, "Search for heavy neutrinos and third-generation leptoquarks in hadronic states of two τ leptons and two jets in proton-proton collisions at $\sqrt{s} = 13$ TeV", *JHEP* **03** (2019) 170, doi:10.1007/JHEP03(2019)170, arXiv:1811.00806.

[59] CMS Collaboration, "Search for supersymmetry in events with a τ lepton pair and missing transverse momentum in proton-proton collisions at $\sqrt{s} = 13$ TeV", *JHEP* **11** (2018) 151, doi:10.1007/JHEP11(2018)151, arXiv:1807.02048.

[60] CMS Collaboration, "Measurement of the differential Drell-Yan cross section in proton-proton collisions at $\sqrt{s} = 13$ TeV", *Submitted to: JHEP* (2018) arXiv:1812.10529.

[61] CMS Collaboration, "Measurements of $\mathrm{t\bar{t}}$ differential cross sections in proton-proton collisions at $\sqrt{s} = 13$ TeV using events containing two leptons", *JHEP* **02** (2019) 149, doi:10.1007/JHEP02(2019)149, arXiv:1811.06625.

[62] CMS Collaboration, "Measurement of the WW cross section pp collisions at sqrt(s)=13 TeV", CMS Physics Analysis Summary CMS-PAS-SMP-16-006, CERN, Geneva, 2016.

[63] CMS Collaboration, "Measurement of top quark pair production in association with a Z boson in proton-proton collisions at $\sqrt{s}$ = 13 TeV", CMS Physics Analysis Summary CMS-PAS-TOP-18-009, CERN, Geneva, 2019.

[64] CMS Collaboration, "Measurement of differential cross sections and charge ratios for t-channel single top quark production at 13 TeV", CMS Physics Analysis Summary CMS-PAS-TOP-17-023, CERN, Geneva, 2019.

[65] CMS Collaboration, "Measurements of the pp $\to$ WZ inclusive and differential production cross section and constraints on charged anomalous triple gauge couplings at $\sqrt{s} = 13$ TeV", *JHEP* **04** (2019) 122, doi:10.1007/JHEP04(2019)122, arXiv:1901.03428.

[66] CMS Collaboration, "Measurement of the differential cross sections for the associated production of a W boson and jets in proton-proton collisions at $\sqrt{s} = 13$ TeV", *Phys. Rev.* **D96** (2017), no. 7, 072005, doi:10.1103/PhysRevD.96.072005, arXiv:1707.05979.

[67] T. Junk, "Confidence level computation for combining searches with small statistics", *Nuclear Instruments and Methods in Physics Research Section A: Accelerators, Spectrometers, Detectors and Associated Equipment* **434** (1999), no. 2, 435 – 443, doi:https://doi.org/10.1016/S0168-9002(99)00498-2.

[68] A. L. Read, "Presentation of search results: the CLs technique", *Journal of Physics G: Nuclear and Particle Physics* **28** (sep, 2002) 2693–2704, doi:10.1088/0954-3899/28/10/313.

[69] The ATLAS Collaboration, The CMS Collaboration, The LHC Higgs Combination Group Collaboration, "Procedure for the LHC Higgs boson search combination in Summer 2011", CMS Physics Analysis Summary CMS-NOTE-2011-005. ATL-PHYS-PUB-2011-11, CERN, Geneva, Aug, 2011.

[70] G. Cowan, K. Cranmer, E. Gross, and O. Vitells, "Asymptotic formulae for likelihood-based tests of new physics", *Eur. Phys. J.* **C71** (2011) 1554, doi:10.1140/epjc/s10052-011-1554-0, 10.1140/epjc/s10052-013-2501-z, arXiv:1007.1727. [Erratum: Eur. Phys. J.C73,2501(2013)].